Structure of a Mesomorphic Polymer: Poly(hexamethylene 4,4′-biphenyldicarboxylate). 2. The Polymer

Xiaodong Li and François Brisse*

Département de Chimie, Université de Montréal, C.P. 6128, Succursale A, Montréal, Québec, Canada H3C 3J7

Received February 16, 1994; Revised Manuscript Received August 10, 1994®

ABSTRACT: The title polymer, P6BP, was studied by X–ray fiber diffraction and differential scanning calorimetry. Three solid crystalline forms (α, β, and γ) and the mesophase S_A were observed. The transformation temperatures are α- to β-form (200–208 °C), β- to γ-form (210–216 °C), γ-form to S_A (216 °C), and S_A to isotropic liquid (227 °C). The three crystalline forms belong to the monoclinic system. The unit-cell dimensions are a = 10.98 Å, b = 11.47 Å, c = 19.62 Å, and β = 89.7° (α-form); a = 13.39 Å, b = 12.84 Å, c = 39.19 Å, and β = 84.7° (β-form); a = 9.70 Å, b = 9.20 Å, c = 19.39 Å, and β = 83.0° (γ-form). The structures of the α- and γ-forms were established using the model compounds' structural information which was obtained in the first part of this work. The polymer chains in the α- and γ-forms are composed of the aliphatic sequences in the *all-trans* conformation, but the dihedral angles formed between the aromatic rings of the biphenyl groups are 40 and 19°, respectively. The unit cell of the α-form contains six chains which are packed in the "face-to-face" pattern with respect to the aromatic groups. The four chains in the unit cell of the γ-form pack in the herringbone pattern. The chain arrangements in the β-form and in the S_A mesophase are also proposed. An abnormal phenomenon in the diffraction pattern, preferred tilt of the c-axis related to fiber, was found in the γ- and α-forms, which was described quantitatively and explained.

Introduction

In order to investigate the structure of the mesomorphic polymer, poly(hexamethylene 4,4′-biphenyldicarboxylate) (P6BP), two model compounds, di-*n*-hexyl 4,4′-biphenyldicarboxylate (6BP6) and hexamethylene di-4-biphenylcarboxylate (BP6BP), were analyzed by X-ray single crystal diffractometry. The results of this analysis are described in the first part of this work.[1] The structural information taken from the model compounds is the basis for the construction of the chain of P6BP. In addition, the packing modes adopted by the compounds also throw a light on the way the polymer chains are possibly arranged.

In the last 10 years, P6BP and its analogues have been investigated for their academic interest[2–9] and their application as high strength materials.[10] The only mesophase was shown to be S_A. Various techniques were employed in these studies: microscopy,[2,5] mutual miscibility,[4,5] and X-ray diffraction.[4,6–8] The temperatures and the enthalpy differences of the thermal transformations of P6BP were also reported.[2–10] Although the observed melting and clearing temperatures, T_i and T_m, are similar to one another, there are also some small endothermic transformations in the solid state which need to be explained. The groups of Krigbaum[4] and Watanabe[6,7] reported the fiber repeat of P6BP in the S_A phase as 18.7 and 18.3 Å, respectively. Krigbaum *et al.*[4] also recorded the X–ray diffraction pattern of crystalline P6BP. However, probably because of the difficulty in drawing the oriented fibers and in identifying the different unknown crystalline forms in the pattern, the reflections could not be indexed and no unit-cell dimensions were reported. Following an electron microscopic study, Takahashi and Nagata[11] concluded that, in the mesophase, P6BP is composed of folded-chain spherulites with lamellae about 250 Å thick.

In this work, the various crystalline forms of P6BP are identified and characterized using X-ray fiber diffraction and differential scanning calorimetry. The polymorphism of the polymer is thus established and the structures of two of the three distinct crystalline forms are proposed.

Experimental Section

Synthesis of P6BP. A tube reactor was charged with dimethyl 4,4′-biphenyldicarboxylate, an excess of hexamethylene glycol and a small amount of titanium(IV) isopropoxide. The mixture was stirred under Ar at 185 °C. After 3 h, the temperature was raised gradually to 290 °C when the system became viscous. The pressure was reduced to about 1 mmHg in order to remove the methanol and the excess diol. The product was white and crisp, and the yield was 85%.

Microscopic Observations. The phase changes of P6BP were observed with a Leitz microscope under crossed polarizers. The polymer started to turn to the characteristic smectic focal-conic texture at about 216 °C (T_m). The texture is very similar to that shown in published reports.[2,4] When the temperature was raised to T_i = 227 °C, the mesophase became a clear isotropic liquid.

Viscosity and Density Determinations. A 5 g/L solution of the polymer was prepared in a 60/40 (w/w) mixture of phenol and tetrachloroethane.[4,8] The inherent viscosity of P6BP, η_{inh}, determined at 25.0 °C with an Ubbelohde capillary viscometer was 0.47 dL/g. The density of the amorphous polymer was measured by flotation in an aqueous solution of $ZnCl_2$ and was found to be 1.22 g/cm^3.

Differential Scanning Calorimetry. DSC measurements were performed using the Perkin-Elmer DSC-1B apparatus. The scanning rate was 20 °C/min for heating, while for cooling, the rate varied.

X-ray Diffraction of P6BP. Thin P6BP fibers, with an average diameter of about 0.05 mm, were drawn from the isotropic melt at 250 °C. The fibers were then stretched and annealed. The diffraction patterns were recorded with a Philips X-ray generator using nickel-filtered Cu Kᾱ radiation and a flat film Warhus camera. The fiber-to-film distance was about 47 mm and was calibrated using NaF standard powder.

Structure Determination of P6BP. The unit-cell dimensions and the indexing of the reflection spots were obtained by a trial and error method. The intensities of the reflection spots

* To whom all correspondence may be addressed.

® Abstract published in *Advance ACS Abstracts,* November 1, 1994.

0024-9297/94/2227-7725$04.50/0

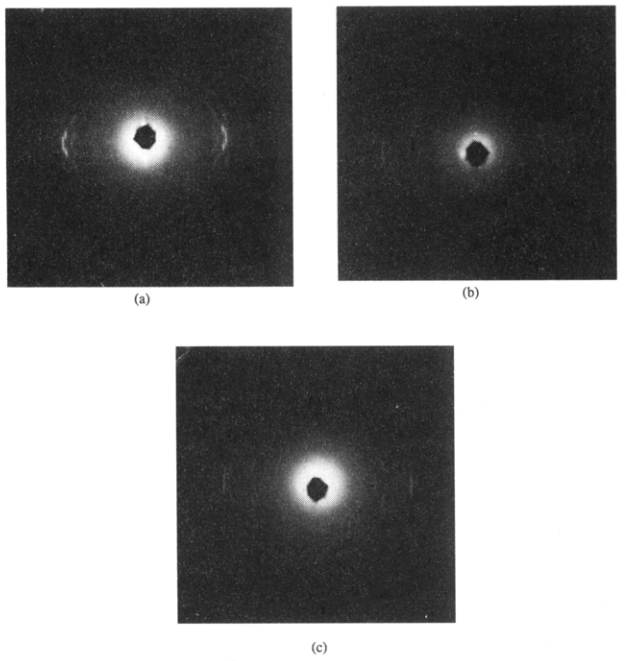

Figure 1. P6BP's diffraction films from (a) fiber stretched at 150 °C (the γ-form and a small fraction of the β-form); (b) fiber stretched and annealed at 190 °C for 2 days (the α-form and a small fraction of the β-form); (c) fiber as in (b) annealed for 1 more week and stretched some more (pure α-form).

were visually estimated on a relative scale of 0−100. Up to 12 observers evaluated the intensites which were then averaged. There was a surprisingly good agreement among the various observations. The observed structure factors, $|F_o|$'s, were calculated from the intensity measurements after Lorentz and polarization corrections were applied.

The bond distances, bond angles, and torsion angles of the two model compounds[1] were used to build an initial monomer chain. Thus, the chain has a fiber repeat which almost matches the experimental c-dimension. The chain was then translated and rotated within the unit cell in order to minimize the packing interactions. The structure factors, $|F_c|$'s, were calculated using the atomic coordinates corresponding to the best position of the chains in the unit cell. The scale factor and an overall isotropic thermal parameter were refined. In the course of the refinement, some slight conformational changes were applied in order to improve the $|F_o| - |F_c|$ agreement. The bond distances and bond angles were also subjected to minor modifications to make the length of the structure repeat exactly fit the c-axis of the unit cell.

Results and Discussion

1. Observation and Identification of the Three Crystalline Forms of P6BP. The first diffraction film of P6BP fiber, which was stretched at 150 °C, is shown in Figure 1a. This pattern is composed of more than one crystalline form, and no reasonable unit cell, taking into account all the diffraction spots, could be deduced. By annealing this fiber at about 190 °C (just before the fiber breaks by partial melting) for 2 days, a completely different diffraction pattern emerged. It is shown in Figure 1b. However, this still did not give a unique unit cell. When the fibers were annealed for another 2 weeks or longer and stretched some more, the pattern shown in Figure 1c was obtained.

All the reflection spots in Figure 1c correspond to a pure crystalline form and could all be indexed with a monoclinic unit cell of dimensions $a = 10.98$ Å, $b = 11.47$ Å, $c = 19.62$ Å, and $\beta = 89.7°$. The comparison of the observed and the calculated d-spacings is given in Table 2. Since this form cannot be reached directly from the melt but only after a long annealing time, it is considered to be the low-temperature phase and is called the α-form.

Table 1. Crystal Data of Interest for the Three Forms of P6BP

parameter	α-P6BP	β-P6BP	γ-P6BP
monomer formula	$C_{20}H_{20}O_4$	$C_{20}H_{20}O_4$	$C_{20}H_{20}O_4$
monomer mol wt	324.4	324.4	324.4
transition temp, °C	200−208	210−216	216
λ (Cu Kα), Å	1.541 78	1.541 78	1.541 78
unit cell	monoclinic	monoclinic	monoclinic
a, Å	10.98	13.39	9.70
b, Å	11.47	12.84	9.20
c, Å	19.62	39.19	19.39
β, deg	89.7	84.7	83.0
V, Å^3	2471	6709	1717
Z	6	16	4
chains/unit cell	6	8	4
d_o(amorphus), g cm^{-3}	1.22	1.22	1.22
d_c, g cm^{-3}	1.307	1.284	1.254
space group	$P2_1$		$P2_1$
h,k,l ranges	$-3 \le h \le 3$	$-5 \le h \le 5$	$-2 \le h \le 2$
	$0 \le k \le 2$	$0 \le k \le 3$	$0 \le k \le 3$
	$0 \le l \le 6$	$0 \le l \le 14$	$0 \le l \le 6$
no. of unique diffraction spots	15	16	31
$R = \Sigma\|\Delta F\|/\Sigma\|F_0\|$, %	15.1		18.4

Table 2. Comparison of Calculated and Observed d-Spacings, ζ's, and Structure Factors for α-P6BP

spot no.	hkl	d_c, Å	d_o, Å	ζ_c, Å^{-1}	ζ_o, Å^{-1}	$\|F_{c,ref}\|$	$\|F_c\|^a$	$\|F_o\|$
1	020	5.737	5.75	0.0012	0.0	2.639	2.639	2.97
2	300	3.660	3.66	0.0095	0.0	5.555	5.555	4.74
3	310	3.487	3.49	0.0101	0.0	1.934	1.934	1.95
4	230	3.138	3.08	0.0082	0.0	1.804	1.804	1.81
5	001	19.620	19.45	0.0509	0.051	1.515	1.515	1.77
6	111	7.365	7.34	0.0547	0.055	1.504	1.735	1.49
	$\bar{1}11$	7.345		0.0484		0.865		
7	121	4.925	4.93	0.0553	0.056	3.565	3.593	3.27
	$\bar{1}21$	4.919		0.0490		0.444		
8	$\bar{2}21$	3.885	3.89	0.0458	0.045	2.451	2.585	3.21
	221	3.891		0.0585		0.822		
9	$\bar{1}02$	7.297	7.33	0.0987	0.098	1.018	1.075	1.97
	102	7.335		0.1050		0.269		
	012	7.457		0.1024		0.216		
10	$\bar{1}22$	4.510	4.51	0.0999	0.102	2.063	2.183	2.64
	122	4.519		0.1062		0.570		
11	$\bar{2}22$	3.682	3.71	0.1094	0.107	1.552	1.557	1.67
	$\bar{2}22$	3.673		0.0967		0.125		
12	232	2.992	2.99	0.1100	0.102	0.356	1.093	1.08
	$\bar{2}32$	2.987		0.0973		0.441		
	322	2.947		0.1126		0.698		
	$\bar{3}22$	2.940		0.0935		0.622		
13	$\bar{1}24$	3.535	3.54	0.2081	0.206	0.948	1.021	0.84
	$\bar{1}24$	3.526		0.2017		0.378		
14	105	3.702	3.68	0.2578	0.253	0.435	0.607	0.94
	$\bar{1}05$	3.689		0.2515		0.126		
	015	3.713		0.2553		0.405		
15	026	2.841	2.84	0.3068	0.303	0.721	0.986	0.78
	206							
	206	2.803		0.2992		0.573		
	$\bar{2}06$	2.816		0.3119		0.351		

[a] $F_c = (\Sigma F_{c,ref}^2)^{1/2}$ for overlapping reflections.

The majority of the diffraction spots in Figure 1a can be indexed with a monoclinic unit cell of dimensions $a = 9.70$ Å, $b = 9.20$ Å, $c = 19.39$ Å, and $\beta = 83.0°$. The comparison of the d-spacings is given in Table 3. In this pattern, most of the diffraction spots deviate somewhat from the layer lines (this point will be discussed later). After a prolonged annealing time, this γ-form tends to decrease in intensity. Thus it is considered the highest-

Table 3. Comparison of Calculated and Observed *d*-Spacings, ζ's, and Structure Factors for γ-P6BP

spot no.	*hkl*	d_c, Å	d_o, Å	ζ_c, Å^{-1}	ζ_o, Å^{-1}	$\lvert F_{c,ref}\rvert$	$\lvert F_c\rvert^a$	$\lvert F_o\rvert$
1	100	9.625	9.61	0.0119	0.012	0.653	0.653	0.68
2	110	6.651	6.61	0.0119	0.011	1.742	1.742	0.87
3	200	4.812	4.83	0.0239	0.024	1.855	2.247	1.82
	201	4.809		0.0281		1.268		
4	020	4.601	4.58	0.0000	0.000	2.397	2.397	2.10
5	210	4.264	4.27	0.0239	0.027	2.762	3.550	4.00
	211	4.262		0.0281		2.231		
6	120	4.151	4.12	0.0119	0.000	3.334	3.334	4.00
7	220	3.325	3.31	0.0239	0.027	2.451	2.451	2.44
8	300	3.208	3.22	0.0358	0.032	0.800	0.800	0.80
9	130	2.922	2.89	0.0119	0.012	0.758	0.758	1.02
10	001	19.247	19.31	0.0519	0.052	2.583	2.583	3.18
11	$\bar{1}01$	9.064	9.02	0.0400	0.041	0.821	0.821	0.93
12	$\bar{1}01$	8.215	8.22	0.0639	0.063	0.746	0.746	0.65
13	111	6.457	6.45	0.0400	0.040	2.514	2.514	1.52
14	$\bar{1}11$	6.128	6.13	0.0639	0.065	1.242	1.242	0.73
15	$\bar{2}01$	4.540	4.53	0.0758	0.077	3.634	3.634	3.89
16	021	4.474	4.46	0.0519	0.054	1.619	1.619	1.82
17	$\bar{2}11$	4.071	4.05	0.0758	0.078	1.913	1.913	1.74
18	$\bar{1}21$	4.014	4.01	0.0639	0.063	2.175	2.175	2.93
19	311	3.047	3.04	0.0161	0.013	1.330	1.330	1.35
20	131	2.905	2.89	0.0639	0.066	1.525	1.525	1.59
21	002	9.623	9.54	0.1039	0.105	0.948	0.948	1.36
22	012	6.650	6.63	0.1039	0.104	0.416	0.416	0.60
23	$\bar{1}12$	5.267	5.26	0.1158	0.117	0.875	0.875	1.00
24	$\bar{2}02$	4.108	4.11	0.1278	0.128	1.854	1.854	2.00
25	$\bar{1}22$	3.740	3.73	0.1158	0.119	0.370	1.180	1.27
	213	3.744		0.1319		1.120		
26	003	6.416	6.38	0.1558	0.157	0.497	0.497	0.72
27	013	5.263	5.26	0.1558	0.157	0.510	0.510	0.93
28	$\bar{2}14$	3.032	3.03	0.2316	0.231	0.403	0.785	0.63
	215	3.025		0.2358		0.673		
29	015	3.551	3.55	0.2597	0.262	1.121	1.121	1.00
30	$\bar{1}15$	3.216	3.24	0.2716	0.272	0.429	0.429	0.90
31	$\bar{2}15$	2.715	2.70	0.2836	0.290	0.223	0.418	0.68
	216	2.709		0.2878		0.353		

[a] $F_o = (\Sigma F_{c,ref}^2)^{1/2}$ for overlapping reflections.

Table 4. Comparison of Observed and Calculated *d*-Spacings of β-P6BP

spot no.	*hkl*	d_c, Å	d_o, Å
1	020	6.421	6.39
2	130	4.075	4.06
3	$\bar{1}21$	5.689	5.63
4	321	3.664	3.66
5	$\bar{1}22$	5.486	5.47
6	$\bar{3}02$	4.248	4.30
7	$\bar{1}23$	5.208	5.16
8	503	2.661	2.66
9	$\bar{5}03$	2.566	2.56
10	$\bar{1}14$	6.506	6.50
11	$\bar{2}25$	3.871	3.90
12	218	3.925	3.91
13	1,1,10	3.681	3.69
14	$\bar{1}$,1,10	3.515	3.50
15	0,0,12	3.252	3.29
16	0,1,14	2.724	2.72

temperature phase which is directly transformed into the mesophase upon heating.

The diffraction spots that do not belong to either the γ-form in Figure 1a or to the α-form in Figure 1b constitute another crystalline form: the β-form. These spots were also indexed with a monoclinic unit cell of dimensions $a = 13.39$ Å, $b = 12.84$ Å, $c = 39.19$ Å, and $\beta = 84.7°$. The observed and calculated d-spacings are compared in Table 4. Since some of the spots in this intermediate form overlap some of the strong ones of either the α- or γ-forms, their intensities were not evaluated.

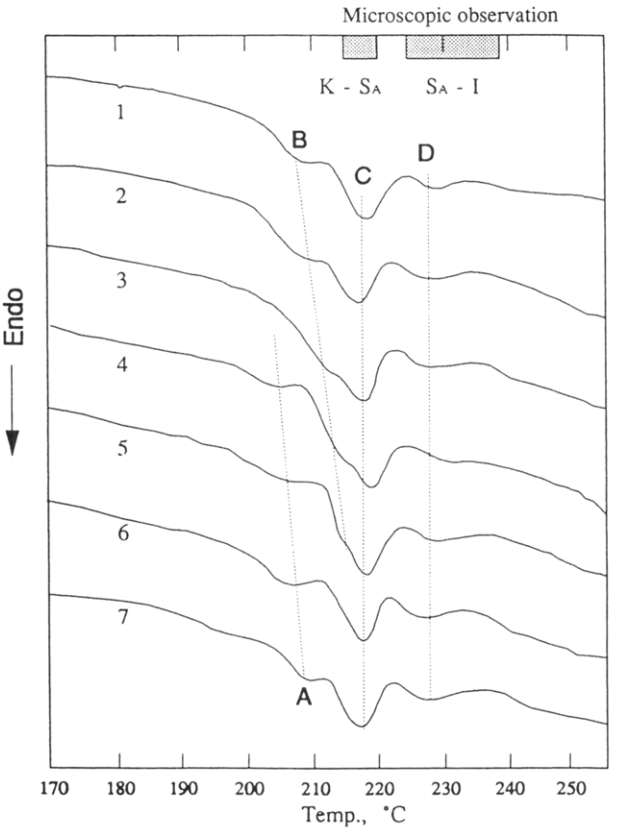

Figure 2. DSC profiles of P6BP. Heating rate: 20 °C/min. (1) Powdered raw P6BP fiber; (2) and (3–6) resins cooled from the isotropic melt at rates of 40, 20, 10, 5, and 2.5 °C/min, respectively; (7) powder of α-P6BP fiber.

In summary, the evolution of the X-ray diffraction patterns reveal that the original γ-phase is transformed into the β-phase which, upon a longer annealing time, turns into the α-phase.

In the DSC profiles shown in Figure 2, there are generally four endothermic peaks. Referring to the observed T_m (216 °C) and T_i (227 °C), the A, B, C, and D peaks are associated with the $\alpha \rightarrow \beta$, $\beta \rightarrow \gamma$, $\gamma \rightarrow S_A$, and $S_A \rightarrow I$ phase transformations, respectively, and the existence of three crystalline forms is confirmed. Figure 2 also shows that, when the resin sample is prepared from the cooled melt at higher and higher cooling rates (the raw fibers is actually a quenched resin), peak A is less and less important and seems to disappear. This is consistent with the fact that the α-phase is not found in the raw fibers because of the supercooling of the high-temperature phases. Although one expects that a high cooling rate would yield more of the γ-form than of the β-form, the convergence of peaks B and C indicates that the two forms cannot be completely separated. The displacement of both the A and B peaks to lower temperatures, as the cooling rate increases, is the consequence of the crystal-to-crystal transformation occurring at a lower temperature when the crystallinity is reduced.

The comparison of the d-spacings and the relative intensities of the diffraction spots to those reported by Krigbaum[4] for unoriented fibers in different states (Table 5) clearly indicates that the slowly cooled fiber is the pure α-form, the fiber annealed after quenching is a mixture of mainly the α- and β-forms, while the quenched fiber is mostly composed of the γ- and β-forms.

2. Preferred Tilt. Figure 3 shows schematically the diffraction patterns of the three crystalline forms. The

Table 5. Comparison of *d*-Spacings and Intensities of P6BP in Different States and Forms

Krigbaum's observation[4]			this work		
slowly cooled from 190 °C	annealed at 190 °C	quenched from 190 °C	α-P6BP	β-P6BP[a]	γ-P6BP[a]
	18.8 (m)[b]	18.7 (s)[b]	19.45 (9)[c]		19.31 (1)[c]
					9.54 (12)
7.31 (m)	7.92 (w)		7.33 (6)		7.34 (11)
					6.63 (13)
		6.47 (w)			6.45 (8)
	6.11 (vvw)			6.39	
5.72 (m)	5.72 (w)		5.75 (4)	5.63	
	5.51 (m)	5.52 (w)		5.47	
	5.12 (m)	5.14 (w)		5.16	
4.92 (s)	4.89 (m)		4.93 (2)		
4.51 (m)	4.49 (w)	4.51 (w)	4.51 (5)		4.58 (6)
					4.53 (4)
					4.46 (9)
		4.21 (m)		4.30	4.27 (3)
				4.06	4.12 (2)
					4.12 (14)
					4.11 (10)
					4.05 (11)
					4.01 (5)
3.89 (m)	3.87 (m)		3.89 (3)	3.90	
				3.91	
3.67 (s)	3.63 (s)	3.68 (w)	3.66 (1)	3.69	3.75 (15)
			3.68 (13)	3.66	
			3.71 (10)		
3.50 (w)	3.48 (vw)		3.54 (14)	3.50	
			3.49 (7)		
		3.32		3.29	3.31 (7)
3.10 (w)	3.08 (vvw)		3.08 (8)		
3.01 (vw)			2.99 (12)		

[a] Intense spots and the spots with *d*-spacing larger than 3 Å only. [b] Intensity: s = strong; m = medium; w = weak; v = very. [c] Relative intensity (1 = the strongest; 2 = the second strongest, ...).

spots of γ-P6BP in Figure 3c do not form well-defined layer lines. This is also true, but to a lesser extent, for some of the spots of the α-P6BP pattern (Figure 3a). This phenomenon has been observed and explained by Daubeny[12] and other authors[13-16] as being due to the tilt of the *c*-axis of the unit cell with respect to the fiber axis in a preferred direction. Stambaugh *et al.*[17] suggested a quantitative equation involving many variables. In this work, this phenomenon is termed the "preferred tilt" in order to distinguish it from the random tilt which is the normal or common situation where the *c* and fiber axes are on the average parallel to one another. In order to understand the preferred tilt and to index the reflection spots of the films, it is necessary to make some theoretical considerations, and the following calculation is proposed.

Preferred tilt is defined, as shown in Figure 4a, as that of a system where the a^* or (and) b^* axis is tilted from the equatorial plane. Consequently, the reflection spots do not remain on layer lines but are slightly displaced above and below it. In general, the orientation of the a^*, b^*, and c^* axes is defined by the ϕ_a, ϕ_b, and ϕ_c angles with respect to the *F*-axis (which is parallel to the fiber and passes through the origin of the reciprocal lattice). A given reflection spot, *hkl*, will take the ζ value represented by eq 1.

$$\zeta_{hkl} = ha^* \cos \phi_a + kb^* \cos \phi_b + lc^* \cos \phi_c \quad (1)$$

In a non-preferred-tilt system, ϕ_a and ϕ_b are equal to 90°; therefore, $\zeta_{hkl} = lc^* \cos \phi_c = l/c$.

In a flat film, as shown in Figure 4b, the observed normal distance of a reflection spot to the equator, Y_{hkl}, is the projection of ζ_{hkl}. These quantities are related through the following equation:

$$Y_{hkl} = 2D\lambda d_{hkl}^2 \zeta_{hkl}/(2d_{hkl}^2 - \lambda^2) \quad (2)$$

where *D* is the fiber-to-film distance, d_{hkl} is the *d*-spacing, and λ is the wavelength of the X-radiation.

For a system with *n* reflections, the preferred-tilt angles can be calculated by solving the following set of overdetermined linear equations:

$$\begin{bmatrix} h_1a^* & k_1b^* & l_1c^* \\ h_2a^* & k_2b^* & l_2c^* \\ \cdots & \cdots & \cdots \\ h_na^* & k_nb^* & l_nc^* \end{bmatrix} \begin{bmatrix} \cos \phi_a \\ \cos \phi_b \\ \cos \phi_c \end{bmatrix} = (1/2\lambda D) \begin{bmatrix} (2 - \lambda^2/d_1^2)Y_1 \\ (2 - \lambda^2/d_2^2)Y_2 \\ \cdots \\ (2 - \lambda^2/d_n^2)Y_n \end{bmatrix} \quad (3)$$

In fact, only two of the three preferred-tilt angles are independent. The third, say ϕ_c, is a function[18] of the α, β, γ, ϕ_a, and ϕ_b quantities:

$$\sin^2 \gamma^* \cos^2 \phi_c + 2[\cos \phi_b(\cos \beta^* \cos \gamma^* - \cos \alpha^*) + \cos \phi_a(\cos \alpha^* \cos \gamma^* - \cos \beta^*)] \cos \phi_c + [(\cos \alpha^* \cos \beta^* - \cos \gamma^* + \cos \phi_a \cos \phi_b)^2 + (\cos \beta^* \sin \phi_b + \cos \alpha^* \sin \phi_a)^2 - (\cos \alpha^* \cos \beta^* + \sin \phi_a \sin \phi_b)^2] = 0 \quad (3a)$$

For a preferred-tilt system, the correctness of the assumed *hkl* should be decided not only by the comparison of the observed and calculated *d*-spacings but also by the good agreement between the observed and calculated ζ's. The preferred-tilt angles ϕ_a, ϕ_b, and ϕ_c of α-P6BP were found to be 88.0, 89.6, and 2.3°; while for γ-P6BP, they are 96.6°, 90°, and 0.4°, respectively. The calculated and observed ζ's are listed in Tables 2 and 3, respectively, where the ζ_{cal} is calculated from eq 1 with the above preferred-tilt angles and ζ_{obs} is derived from the observed Y_{obs} and d_{obs}'s by eq 2.

An examination of published fiber patterns reveals that the preferred-tilt situation is present in about 20% of the cases. However, in these cases, the values of ϕ_a and (or) ϕ_b were generally too close to 90° to be of concern, or, with a few exceptions, to be noted.[12-17]

The origin of the preferred tilt is seen as a rearrangement of the polymer chains when the crystalline domains are formed. For example, in the case of an aromatic polymer such as P6BP, the γ-form is produced upon cooling of the S_A mesophase. In this phase, the chains are organized in such a way that (i) the chains are parallel to the fiber axis and (ii) the aromatic groups of different chains form layers normal to the chain direction. In order to fit into the unit cell of the γ-form in which β is acute, the molecular chains cannot meet the above two conditions at the same time. They may adopt one or the other of the two dispositions shown in Figure 5: (a) move along the fiber axis so that the chains remain parallel to the fiber direction or (b) tilt simultaneously relative to the fiber axis in a direction such that the aromatic groups remain normal to the

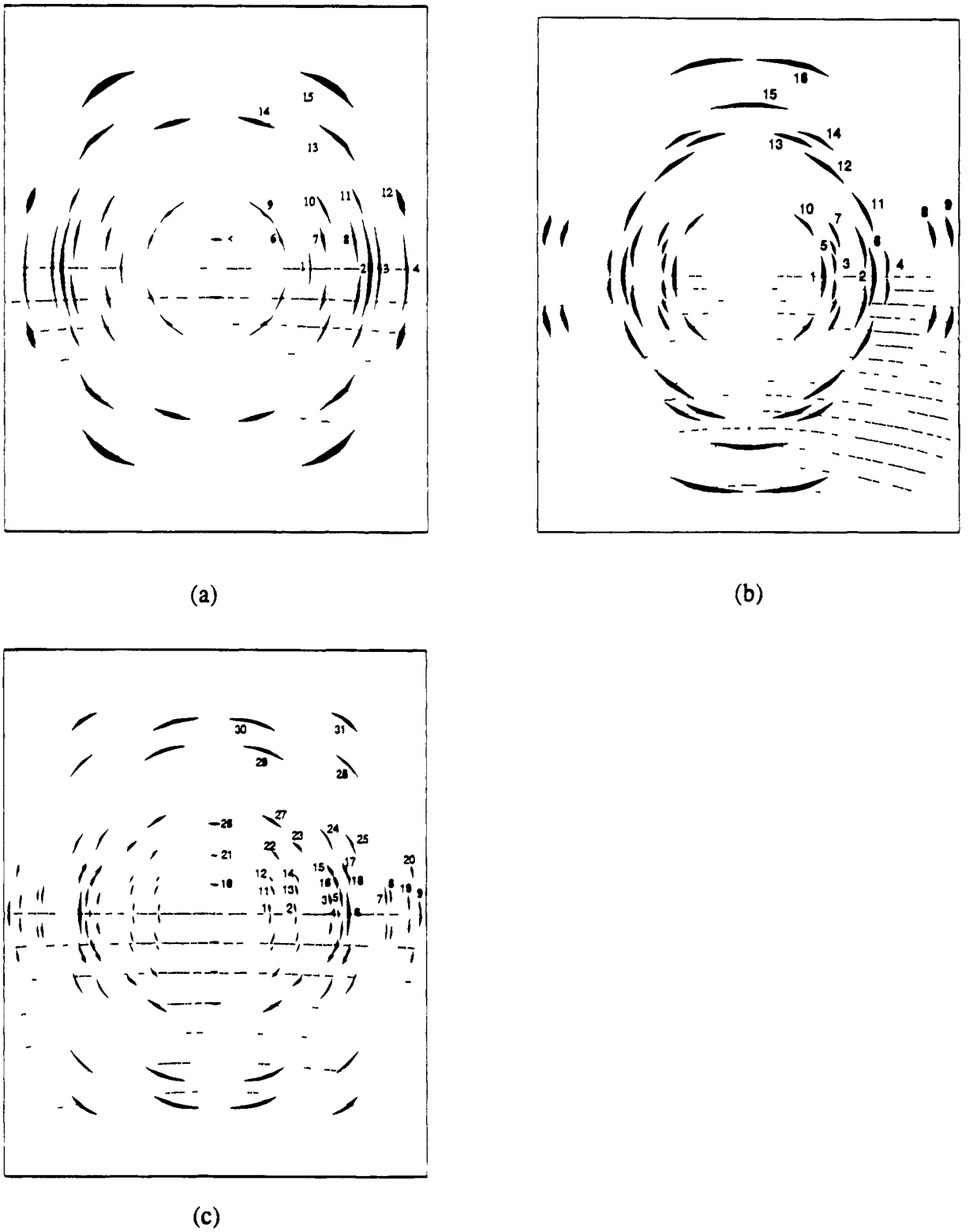

Figure 3. Schematic diffraction patterns of (a) α-P6BP, (b) β-P6BP, and (c) γ-P6BP.

fiber axis. Obviously, the axial translation of a long chain is hindered because of the strong interactions between chains. Therefore, the chains of γ-P6BP will tilt preferably in a direction that causes the angle between the c^* and the fiber axes to decrease from ϕ_{nt}, the angle in the non-preferred-tilt system, to the observed ϕ_c. The ϕ_{nt} can be calculated by the following equation which is derived from eq 3a.

$$\cos \phi_{nt} = (1 - \cos^2 \alpha^* - \cos^2 \beta^* - \cos^2 \gamma^* + 2 \cos \alpha^* \cos \beta^* \cos \gamma^*)^{1/2}/\sin \gamma^* \quad (4)$$

In the case of P6BP in the γ-form, the ϕ_{nt} angle of 7.0° is reduced to ϕ_c of 0.4°.

3. The Polymer Structure. *α-P6BP.* There are three independent monomer chains per unit cell of space group $P2_1$. The refinement of the scale factor and an overall isotropic thermal parameter B = 16.8 Å^2 was concluded when R reached 15.1%. The comparison of the observed and calculated structure factors is shown in Table 2. The individual atomic coordinates are listed in Table 6. The atomic numbering is given in Figure 6. The torsion angles and the dihedral angles are given in

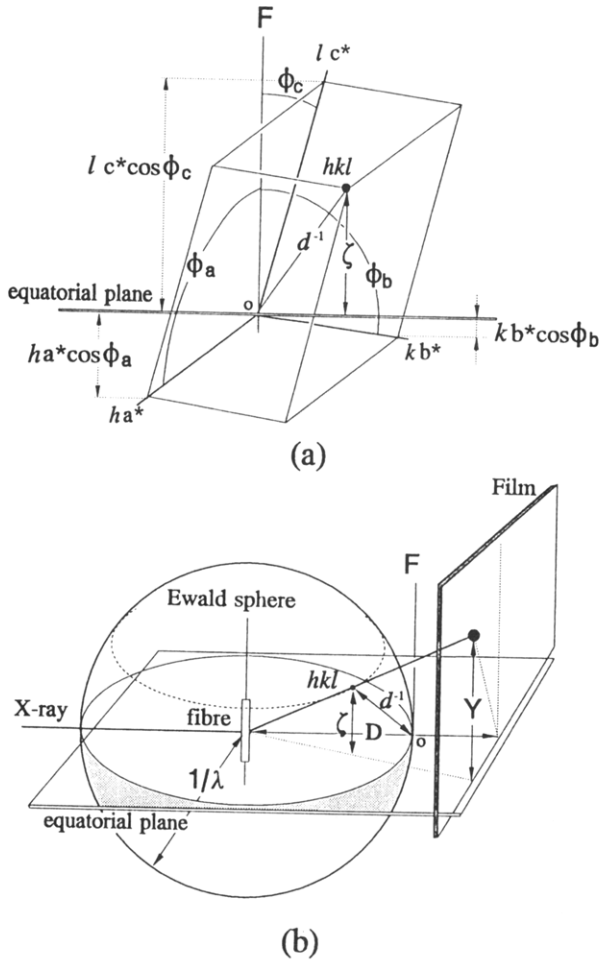

Figure 4. Geometric presentation of a preferred-tilt reciprocal lattice related to the equator plane.

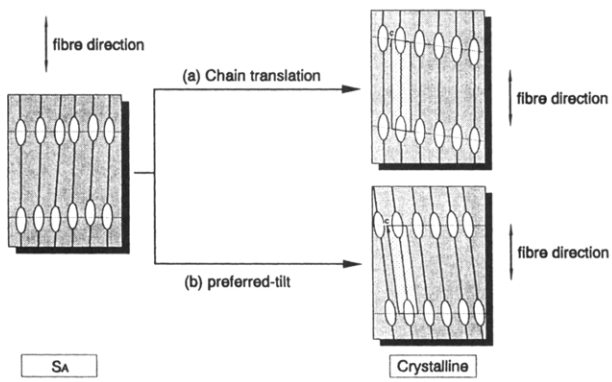

Figure 5. Illustration of the preferred-tilt mechanism.

Table 7. The stereopairs of a single chain and the crystal packing are shown in Figures 7a and 8a, respectively.

The fiber repeat of α-P6BP is 19.62 Å. This is very nearly equal to the calculated fiber repeat for a fully-extended monomer, 19.66 Å. This also compares very well with the corresponding distances in the two model compounds 6BP6 (19.57 (1) Å) and α-BP6BP (19.599 (2) Å).[1] No doubt, the aliphatic sequence of P6BP is in the *all-trans* conformation.

As observed in many benzoates and terephthalates,[1,19–28] the carboxylic group is nearly coplanar with the adjacent aromatic group[27,29–32] and the torsion angle O=C—O—C is in the *cis* conformation.[30,33–35] Furthermore, the two carboxylic groups are in the *E*-conformation, the most frequently observed situation. Geometrically, it is the only possible one in an aromatic polyester with an even number of methylene groups in the *trans* conformation.

The dihedral angle between the two phenyl rings, Φ, was found to be 40°. This observation is in agreement with the theoretical minimum potential barrier.[36–39] The following relationship between the Φ angle and the torsion angle τi's seems to hold true for structures with a single chemical unit in the fiber repeat.

$$\Phi = \sum_i \tau i - (2n+1)\pi \qquad (n = 0, 1, 2, ...) \qquad (5)$$

Thus, for an aromatic polymer crystallizing in the $P\bar{1}$ space group with one chemical unit, Φ = 0°, since to each τi there is a τi′ such that τi′ = −τi. It is impossible for P6BP's aliphatic sequence to be centrosymmetric (where the right hand of eq 5 would be 180° and the biphenyl group would then be planar) although this frequently occurs in *m*(even)-methylene terephthalates[22,25,40] and α-BP6BP.[1]

As shown in Table 7, the aliphatic torsion angles, τ1 to τ6, are all close to 180°. Therefore, the atoms of the aliphatic sequence in this form are almost coplanar. However, since the torsion angles τi and τi′ all have the same sign, the chain cannot be centrosymmetric. Indeed, a rather large dihedral angle Φ (40°) is observed.

It is notable that, in the case of 6BP6,[1] the molecular chain and the *c* axes are parallel. The perpendicular projection of one molecule onto the *ab* plane has an area $S = {}^1/_2a \times {}^1/_2b = 3.877 \times 5.714$ (Å^2). Such a rectangular area implies that the aromatic groups adopt a face-to-face (FTF) packing pattern. A similar situation is noted for α-P6BP, where the area of the projection of a chain is $S = {}^1/_3a \sin\beta \times {}^1/_2b = 3.66 \times 5.74$ (Å^2). It is clear that the packing pattern of α-P6BP should also be of the FTF type. The "faces" will be roughly parallel to the *bc* plane. As a matter of fact, this similarity of the packing patterns was helpful in solving the structure of α-P6BP.

γ-P6BP. The fiber repeat of γ-P6BP (*p* = 19.39 Å) is slightly shorter than that for a fully-extended conformation. However, as can be seen in Table 8, the aliphatic sequence is still in the *trans* conformation. The structure was refined in the space group $P2_1$, and the final *R* value, 18.4%, was obtained with an overall isotropic thermal parameter of *B* = 11.9 Å^2. The comparison of the structure factors and the final atomic coordinates of the two independent chains present in the unit cell are shown in Tables 3 and 9, respectively. The structure of the chain and the unit-cell content are illustrated in Figures 7b and 8b, respectively.

In this form, the most interesting structural feature is that the torsion angles τ4, τ4′, τ5, and τ5′ (−147, 140, 163, and −163°) are considerably smaller than 180° (Table 7). These smaller torsion angles not only are responsible for the shorter *c*-axis (19.39 Å) but also make the sequence of the γ-form bulkier than that of the α-form. The above torsion angles hold different signs in pairs of τi and τi′. Thus, the chain is relatively close to being centrosymmetric, and, consequently, γ-P6BP has a smaller Φ angle, 19°.

The *a* and *b* dimensions of the γ-form do not have any relation with the cell dimensions of either α-P6BP or the model compounds. Thus, the chains will pack in a quite different way. The area of the perpendicular projection of a chain is: $S = {}^1/_2a \sin\beta \times {}^1/_2b$, or 4.81 × 4.60 (Å^2). This nearly square domain implies that the chain packing is most likely of the herringbone type

Table 6. Atomic Coordinates of α-P6BP

	chain I			chain II			chain III		
atom	*X*	*Y*	*Z*	*X*	*Y*	*Z*	*X*	*Y*	*Z*
O1	0.2231	0.5168	0.2646	0.5665	−0.0165	0.5166	0.9025	−0.0165	0.1636
O2	0.1778	0.3365	0.2994	0.5196	0.1634	0.5514	0.8556	0.1634	0.1984
C1	0.1965	0.3655	0.1814	0.5385	0.1345	0.4334	0.8745	0.1345	0.0804
C2	0.1542	0.2528	0.1705	0.4953	0.2469	0.4223	0.8313	0.2469	0.0695
C3	0.1513	0.2073	0.1049	0.4919	0.2924	0.3569	0.8279	0.2924	0.0039
C4	0.1906	0.2744	0.0502	0.5318	0.2256	0.3022	0.8678	0.2256	−0.0508
C5	0.2328	0.3871	0.0611	0.5750	0.1132	0.3131	0.9110	0.1132	−0.0399
C6	0.2357	0.4327	0.1267	0.5784	0.0677	0.3787	0.9144	0.0677	0.0257
C7	0.2005	0.4161	0.2511	0.5430	0.0840	0.5031	0.8790	0.0840	0.1501
C8	0.1793	0.3765	0.3711	0.5214	0.1235	0.6231	0.8574	0.1235	0.2701
C9	0.1743	0.2708	0.4170	0.5154	0.2291	0.6690	0.8514	0.2291	0.3160
C10	0.1754	0.3041	0.4920	0.5169	0.1958	0.7440	0.8529	0.1958	0.3910
O1′	0.2042	−0.0184	0.7658	0.5428	0.5185	1.0178	0.8788	0.5185	0.6648
O2′	0.1722	0.1644	0.7309	0.5124	0.3354	0.9829	0.8484	0.3354	0.6299
C1′	0.1884	0.1342	0.8489	0.5284	0.3658	1.1009	0.8644	0.3658	0.7479
C2′	0.1545	0.2495	0.8598	0.4955	0.2502	1.1118	0.8315	0.2502	0.7588
C3′	0.1547	0.2951	0.9254	0.4961	0.2046	1.1774	0.8321	0.2046	0.8244
C4′	0.1889	0.2255	0.9802	0.5297	0.2745	1.2322	0.8657	0.2745	0.8792
C5′	0.2229	0.1103	0.9693	0.5626	0.3900	0.2213	0.8986	0.3900	0.8683
C6′	0.2226	0.0646	0.9037	0.5620	0.4356	1.1557	0.8980	0.4356	0.8027
C7′	0.1890	0.0835	0.7793	0.5284	0.4165	1.0313	0.8644	0.4165	0.6783
C8′	0.1709	0.1245	0.6592	0.5108	0.3754	0.9112	0.8468	0.3754	0.5582
C9′	0.1737	0.2302	0.6134	0.5145	0.2697	0.8654	0.8505	0.2697	0.5124
C10′	0.1726	0.1969	0.5384	0.5131	0.3029	0.7904	0.8491	0.3029	0.4374

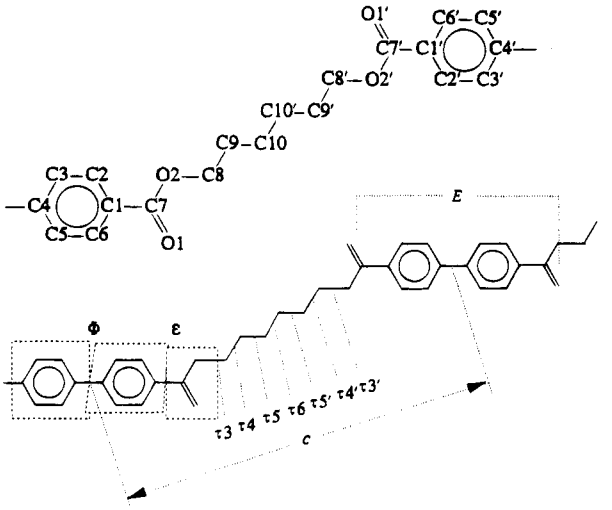

Figure 6. Atomic numbering and conformation definitions of P6BP.

(HB)[41,42] with respect to the aromatic groups. This situation was indeed confirmed by the structure refinement and is shown in Figure 8b.

The packing patterns of the α- and γ-forms are determined by their molecular or chain shapes. For the former, the approximate planar shape favors a parallel packing with the aromatic groups in FTF arrangement, while the aliphatic segments in the bulkier chains of the γ-form are responsible for the herringbone packing pattern. The packing patterns of the α- and γ-P6BP are compared in parts a and c of Figure 9.

β-P6BP. The unit-cell dimensions of β-P6BP were derived from the diffraction pattern schematically illustrated in Figure 3b. The comparison of the calculated and observed *d*-spacings is listed in Table 4. This unit cell is monoclinic, but the *c* dimension, 39.19 Å, is twice the length of a chemical repeat in an extended conformation. The chain structure should resemble those of the α- or γ-form. Taking into account the packings of the α- and γ-forms, the unit-cell dimensions, and the observed *hk*0 reflections, one may propose a believable chain packing for the β-polymorph. The *a* and *b* dimensions are obviously not suitable for FTF packing. However, the diagonal (18.55 Å) is very close to twice the *b*-axis (9.20 Å) of γ-P6BP. Then, it can be assumed that the packing will be of the HB type. Figure 9b displays the proposed packing of β-P6BP.

The Mesophase. When P6BP is cooled down from its S_A phase, the solid crystalline γ-form and a small fraction of the β-form appear fairly quickly, so that the

Table 7. Torsion Angles and Dihedral Angles in α-P6BP and γ-P6BP

		α-P6BP		γ-P6BP	
		unprimed	primed	unprimed	primed
Torsion Angles (deg)					
C6–C1–C7–O2	τ1	170	170	175	175
C1–C7–O2–C8	τ2	179	179	180	180
C7–O2–C8–C9	τ3	171	170	178	178
O2–C8–C9–C10	τ4	180	180	−147	140
C8–C9–C10–C10′	τ5	180	180	163	−163
C9–C10–C10′–C9′	τ6	180		180	
O1–C7–O2–C8		−1	0	1	1
O1–C7–C1–C3		169	168	174	174
O1–C7–C1–C6		−10	−10	−6	−6
O2–C7–C1–C2		−11	−11	−5	−5
C5–C6–C1–C7		179	179	180	180
Dihedral Angles [Plane–Plane] (deg)					
[C1–C2–C3–C4–C5–C6]–[C1′–C2′–C3′–C4′–C5′–C6′]	Φ	−40		−19	
[C1–C2–C3–C4–C5–C6]–[C1–C7(–O1)–O2]	ϵ	9	9	5	5
[C1–C7(–O1)–O2]–[O2–C8–C9–C10–...–O2′]	Ψ	11	15	11	14

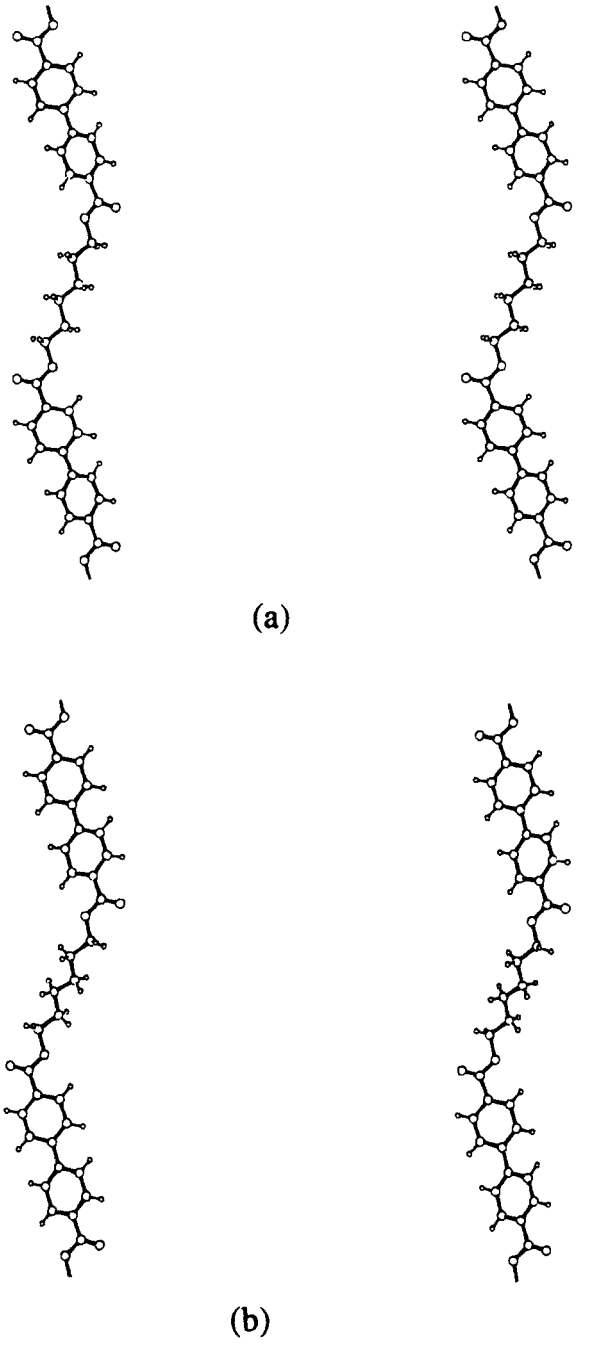

Figure 7. Stereopairs of the polymer chain of (a) α- and (b) γ-P6BP.

conformation and the disposition of the chains in the S_A phase should be close to what it is in the γ-form. Thus, one may assume the structure of the S_A phase by considering the structural changes from α- to γ-form. As the polymer passes through the α-, β-, and γ-forms, the density decreases and the *c*-axis gets shorter (Table 1). Therefore, it is expected that the chains in the S_A phase will pack in a looser manner and that more of the torsion angles in the aliphatic sequences will depart significantly from 180°. This description is supported by the fact that the observed fiber repeat of the S_A form is much smaller, 18.3–18.7 Å,[4,6,7] than that in any of the crystalline phases.

Conclusions

The mesophase polyester, poly(hexamethylene 4,4′-biphenyldicarboxylate) (P6BP), was investigated using X-ray fiber diffraction. The analysis of the polymer's X-ray fiber pattern reveals the existence of three

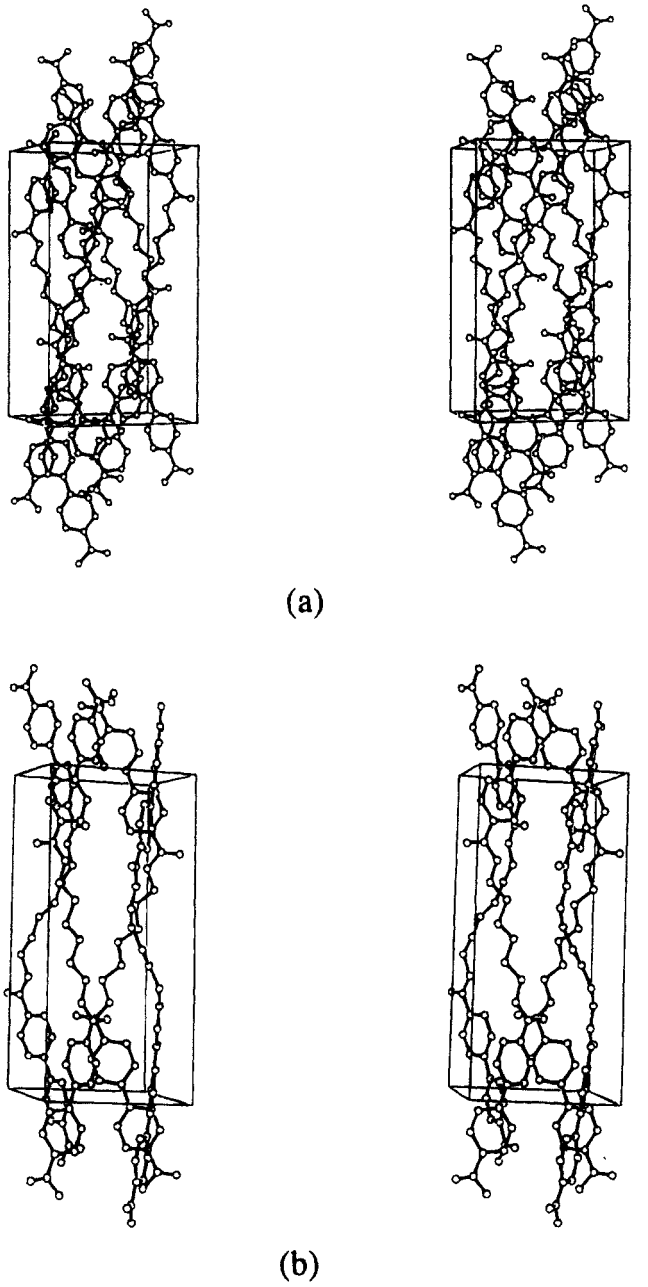

Figure 8. Stereopairs of unit-cell packing of (a) α- and (b) γ-forms.

Table 8. Chain conformation and Calculated Fiber Repeat for P6BP[a]

τ3	τ4	τ5	τ6	τ5′	τ4′	τ3′	fiber repeat, Å	τ3	τ4	τ5	τ6	τ5′	τ4′	τ3′	fiber repeat, Å
t	t	t	t	t	t	t	19.66	g^+	t	t	t	g^+	t	t	18.38
g^+	t	t	t	t	t	t	19.03	g^+	t	t	t	g^-	t	t	18.71
t	g^+	t	t	t	t	t	14.97	g^+	t	t	t	t	t	g^+	18.54
t	t	g^+	t	t	t	t	18.71	g^+	t	t	t	t	t	g^-	18.71
t	t	t	g^+	t	t	t	14.76	t	t	g^+	t	g^+	t	t	18.38
g^+	t	g^+	t	t	t	t	18.54	t	t	g^+	t	g^-	t	t	19.03
g^+	t	g^-	t	t	t	t	19.03								

[a] t, g^+, and g^- represent torsion angle values of +180.0, +60.0, and −60.0°, respectively.

crystalline forms (α, β, and γ) as well as the mesophase S_A. These phases were confirmed by DSC. The α-form is obtained after annealing the raw fiber at 190 °C for a long time. The γ-form is obtained after the fiber is stretched at 150° for a week. The intermediate β-form exists together with the others. The phase transformations are observed at the following temperatures: α →

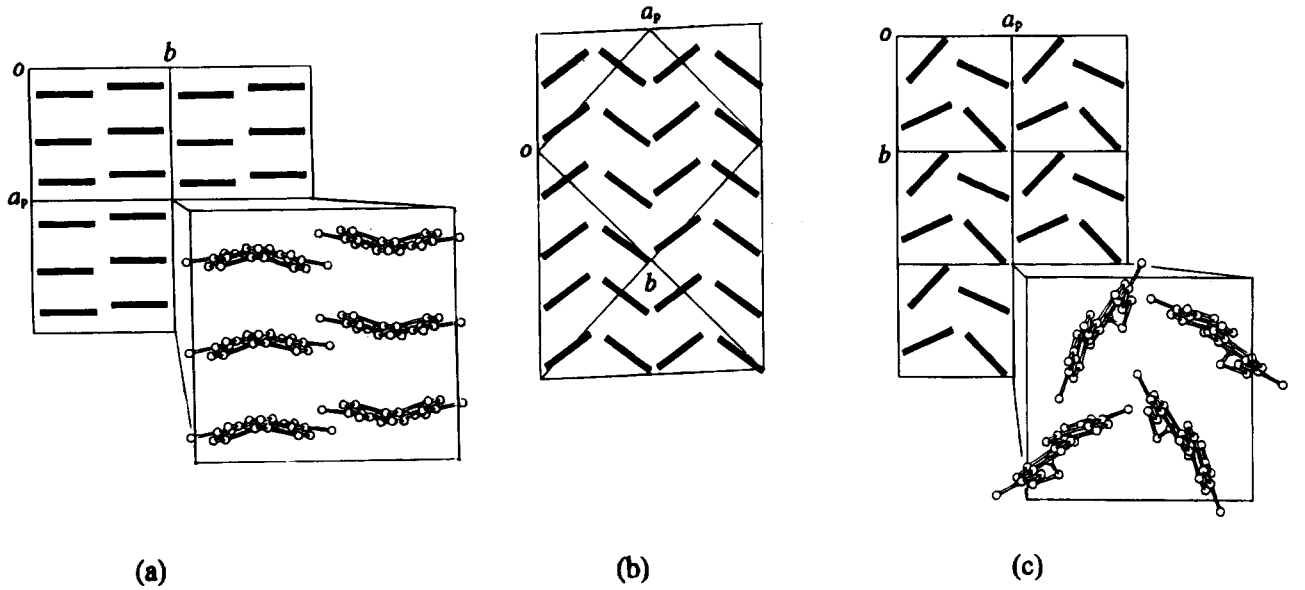

Figure 9. Projection view of the unit cells onto the *ab* plane (a) α-P6BP (b) β-P6BP, and (c) γ-P6BP.

Table 9. Atomic Coordinates of γ-P6BP

	chain I			chain II		
atom	*X*	*Y*	*Z*	*X*	*Y*	*Z*
O1	0.4496	0.0948	0.1631	0.8557	0.5499	0.2378
O2	0.2426	0.1672	0.2173	0.7883	0.3328	0.2834
C1	0.2750	0.1737	0.0951	0.7818	0.3666	0.1636
C2	0.1344	0.2151	0.0952	0.7435	0.2192	0.1575
C3	0.0851	0.2448	0.0295	0.7155	0.1673	0.0905
C4	0.1702	0.2347	−0.0350	0.7244	0.2565	0.0307
C5	0.3097	0.1929	−0.0320	0.7631	0.4028	0.0399
C6	0.3601	0.1636	0.0306	0.7907	0.4558	0.1038
C7	0.3336	0.1413	0.1605	0.8123	0.4282	0.2310
C8	0.2867	0.1398	0.2861	0.8141	0.3792	0.3534
C9	0.1684	0.1822	0.3406	0.7746	0.2551	0.4031
C10	0.2128	0.2436	0.4083	0.7155	0.3010	0.4771
O1′	−0.1352	0.4826	0.7032	0.4901	−0.0652	0.7645
O2′	0.0626	0.3884	0.6471	0.5784	0.1426	0.7151
C1′	0.0277	0.3689	0.7693	0.5974	0.1063	0.8340
C2′	0.1507	0.2854	0.7670	0.6762	0.2357	0.8344
C3′	0.1953	0.2394	0.8318	0.7197	0.2827	0.8992
C4′	0.1222	0.2736	0.8974	0.6877	0.2060	0.9624
C5′	0.0001	0.3573	0.8966	0.6087	0.0775	0.9589
C6′	−0.0454	0.4031	0.8350	0.5653	0.0295	0.8972
C7′	−0.0254	0.4208	0.7045	0.5483	0.0502	0.7689
C8′	0.0244	0.4329	0.5784	0.5362	0.1023	0.6467
C9′	0.1421	0.3892	0.5226	0.5770	0.2258	0.5955
C10′	0.0977	0.3278	0.4549	0.6360	0.1798	0.5215

β (200−208 °C), β → γ (210−216 °C), γ → S_A (216 °C), and S_A → I (227 °C).

The structural features (bond distances, bond angles, the chain conformation, and the packing pattern) of the model compounds 6BP6 and α-BP6BP played an important role in the determination of the polymer's structures. The structure of α-P6BP (monoclinic, $P2_1$) was thus established and confirmed by the good agreement (R = 15.1% for 15 diffraction spots) between observed and calculated structure factors.

The unit cell of the γ-P6BP was established from its diffraction pattern, from which the contribution of the β-form was removed. This form belongs to the monoclinic system, space group $P2_1$. The structure was solved satisfactorily (R = 18.4% for 31 observed diffraction spots) following the same approach.

The diffraction spots of γ- and α-P6BP do not form well-defined layer lines. This phenomenon is associated with the tilt, in a certain direction, of the unit cell's *c*-axis with respect to the fiber axis. The preferred-tilt phenomenon was treated quantitatively and explained. The preferred-tilt angles ϕ_a, ϕ_b, and ϕ_c were calculated to be respectively 96.6°, 90.0°, and 0.4° (γ-P6BP) and 88.0, 89.6, and 2.3° (α-P6BP). The preferred tilt is the consequence of a rearrangement of the chains taking place in the process of crystallization.

The dihedral angle of the biphenyl group is 40° for α-P6BP and is 19° for the γ-form. The conformations of the α- and γ-forms are *all-trans*. All the aliphatic chain torsion angles of the α-form are close to 180°, while in the γ-form, τ4, τ5, τ4′, and τ5′ deviate significantly from 180°. The chain packing of the α-form is characterized by an arrangement of the aromatic groups in a face-to-face pattern, while in the γ-form, the chains are packed in a herringbone pattern.

The β-form of P6BP is monoclinic. It is assumed that the chains are in an *all-trans* conformation and the packing pattern is not too different from that of the γ-form. It is suggested that, in the S_A phase, the torsion angles of the P6BP aliphatic sequences deviate even more from the values reported for the γ-form. It is expected that the chains adopt some kind of herringbone pattern.

Acknowledgment. We acknowledge the financial support of the National Science and Engineering Council of Canada (Grant A-5968).

References and Notes

(1) Li, X.; Brisse, F. *Macromolecules*, preceding paper in this issue.
(2) Meurisse, P.; Noël, C.; Monnerie, L.; Fayolle, B. *Br. Polym. J.* **1981**, *3*, 55.
(3) Krigbaum, W. R.; Asrar, J.; Toriumi, H.; Ciferri, A.; Preston, J. *J. Polym. Sci., Polym. Lett. Ed.* **1982**, *20*, 109.
(4) Krigbaum, W. R.; Watanabe, J. *Polymer* **1983**, *24*, 1299.
(5) Krigbaum, W. R. *J. Appl. Polym. Sci., Appl. Polym. Symp.* **1985**, *41*, 105.
(6) Jackson, W. J., Jr.; Morris, J. C. *J. Appl. Polym. Sci., Appl. Polym. Symp.* **1985**, *41*, 307.
(7) Watanabe, J.; Hayashi, M. *Macromolecules* **1988**, *21*, 278.
(8) Watanabe, J.; Hayashi, M. *Macromolecules* **1989**, *22*, 4083.
(9) Jackson, W. J., Jr.; Morris, J. C. *Polym. Prep. (Am. Chem. Soc., Div. Polym. Chem.)* **1989**, *30*, 489.
(10) Jackson, W. J., Jr.; Morris, J. C. *ACS Symp. Ser.* **1990**, *435*, 16.
(11) Takahashi, T.; Nagata, F. *J. Macromol. Sci., Phys.* **1989**, *B28*, 349.
(12) Daubeny, de P.; Bunn, C. W.; Brown, C. J. *Proc. R. Soc. London* **1954**, *A226*, 531.

(13) Boye, C. A. *J. Polym. Sci.* **1961**, *55*, 275.
(14) Vogelsong, D. C. *J. Polym. Sci.* **1962**, *57*, 895.
(15) Hall, I. H.; Pass, M. G. *Polymer* **1976**, *17*, 807.
(16) Sasaki, S.; Takigawa, S. *J. Polym. Sci.* **1989**, *B27*, 1077.
(17) Stambaugh, B.; Koenig, J. L.; Lando, J. B. *J. Polym. Sci., Polym. Phys. Ed.* **1979**, *17*, 1053.
(18) Li, X. Ph.D. Thesis, Université de Montréal, Montréal, Québec, Canada, 1993.
(19) Bailey, M.; Brown, C. J. *Acta Crystallogr.* **1967**, *B22*, 387.
(20) Krigbaum, W. R.; Barber, P. G. *Acta Crystallogr.* **1970**, *B27*, 1884.
(21) Cobbledick, R. E.; Small, R. W. H. *Acta Crystallogr.* **1972**, *B28*, 2924.
(22) Pérez, S.; Brisse, F. *Can. J. Chem.* **1975**, *53*, 3551.
(23) Sashino, S.; Haisa, M. *Acta Crystallogr.* **1975**, *B31*, 1819.
(24) Brisse, F.; Pérez, S. *Acta Crystallogr.* **1976**, *B32*, 2110.
(25) Pérez, S.; Brisse, F. *Acta Crystallogr.* **1976**, *B32*, 407.
(26) Bocelli, G. *Acta Crystallogr.* **1982**, *B38*, 2072.
(27) Deguire, S.; Gagné, J.; Dugas, H.; Brisse, F. *Can. J. Chem.* **1987**, *65*, 2291.
(28) Hou, J.; Tashiro, K.; Kobayashi, M.; Inoue, T. *J. Phys. Chem.* **1991**, *95*, 9561.
(29) Tonelli, A. E. *J. Polym. Sci., Polym. Lett. Ed.* **1973**, *11*, 441.
(30) Hall, I. H. In *Structure of Crystalline Polymers*; Hall, I. H., Ed.; Elsevier Applied Science: New York, 1984.
(31) Meurisse, D.; Laupretre, F.; Noël, C. *Mol. Cryst. Liq. Cryst.* **1984**, *110*, 41.
(32) Barrio, C.; García-Granda, S.; Gómez-Beltrán, F. *Acta Crystallogr.* **1993**, *C49*, 253.
(33) Hocking, W. H. *Z. Naturforsch.* **1976**, *31A*, 1113.
(34) Blom, C. E.; Günthard, Hs. H. *Chem. Phys. Lett.* **1981**, *84*, 267.
(35) Wiberg, K. B.; Laidig, K. E. *J. Am. Chem. Soc.* **1987**, *109*, 5935.
(36) Bastiansen, O.; Samdal, S. *J. Mol. Struct.* **1985**, *128*, 115.
(37) Häfelinger, G.; Regelman, C. *J. Comput. Chem.* **1987**, *8*, 1057.
(38) Kendrick, J. *J. Chem. Soc., Faraday Trans.* **1990**, *86*, 3995.
(39) Brock, C. P.; Minton, R. P. *J. Am. Chem. Soc.* **1989**, *111*, 4586.
(40) Pérez, S.; Brisse, F. *Acta Crystallogr.* **1977**, *B33*, 1673.
(41) Gavezzoti, A.; Desiraju, G. R. *Acta Crystallogr.* **1988**, *B44*, 427.
(42) Bernstein, J.; Sarma, J. A. R. P.; Gavezzoti, A. *Chem. Phys. Lett.* **1990**, *174*, 361.